PHYSICS

Fractional Coulomb blockade for quasi-particle tunneling between edge channels

Marc P. Röösli[1]*, Michael Hug[1], Giorgio Nicolí[1], Peter Märki[1], Christian Reichl[1], Bernd Rosenow[2], Werner Wegscheider[1], Klaus Ensslin[1], Thomas Ihn[1]

In the fractional quantum Hall effect, the elementary excitations are quasi-particles with fractional charges as predicted by theory and demonstrated by noise and interference experiments. We observe Coulomb blockade of fractional charges in the measured magneto-conductance of a 1.4-micron-wide quantum dot. Interaction-driven edge reconstruction separates the dot into concentric compressible regions with fractionally charged excitations and incompressible regions acting as tunnel barriers for quasi-particles. Our data show the formation of incompressible regions of filling factors 2/3 and 1/3. Comparing data at fractional filling factors to filling factor 2, we extract the fractional quasi-particle charge $e^*/e = 0.32 \pm 0.03$ and 0.35 ± 0.05. Our investigations extend and complement quantum Hall Fabry-Pérot interference experiments investigating the nature of anyonic fractional quasi-particles.

INTRODUCTION

Large quantum dots (QDs) can be used to study physical processes in the quantum Hall regime. Nevertheless, no effects of quasi-particle tunneling have been observed for Coulomb blockaded QDs in the fractional quantum Hall regime so far (*1*). The reason is that tunneling barriers connecting a QD in the Coulomb blockade to source and drain regions are strongly backscattering and therefore only allow for electron tunneling (*2*). Operating barriers in the regime of weak backscattering allows for quasi-particle tunneling. Evidence for fractionally charged quasi-particles has previously been observed in experiments on shot noise of a quantum point contact (*3*–*7*), capacitively probed localized states (*8*), anti-dots (*9*), photo-assisted shot noise (*10*, *11*), or quantum Hall Fabry-Pérot interferometers (*12*). In general, quantum Hall Fabry-Pérot interferometer experiments (*13*–*17*) in the fractional quantum Hall regime offer the opportunity to study anyonic statistics of fractional quasi-particles (*12*, *18*–*27*). Anyonic fractional statistics were recently detected in two seminal experiments by Bartolomei *et al.* (*28*) and by Nakamura *et al.* (*29*). Mach-Zehnder interferometers in the quantum Hall regime (*30*) were proposed as an alternative probe to study quasi-particle statistics (*31*, *32*). The close relation between QDs and Fabry-Pérot interferometers in the quantum Hall regime (*33*–*37*) promises complementary experimental observations on fractional quasi-particles in QDs.

Here, we study the magneto-transport through a large QD containing roughly 900 electrons in the fractional quantum Hall regime for filling factors $\nu < 1$. The QD forms concentric compressible regions separated by incompressible regions (*38*). In the integer quantum Hall regime, this has been established by experiments (*39*–*42*) and theory (*43*). By reconstructing the charge carrier distribution in the QD at zero magnetic field, we can show that in two specific regions of magnetic field, the incompressible region corresponds to a fractional filling factor $\nu_{in} = 1/3$ or $2/3$, respectively. In our experiments, the QD is weakly tunnel-coupled to its leads and occupied by an integer number of electrons N. In this regime, conductance peaks arise each time the chemical potential of the Nth electron state and the leads are degenerate, as usual in Coulomb blockade experiments. While only an integer number of electrons can tunnel between the QD and the leads (*2*), we observe fractional quasi-particle tunneling between the compressible regions inside the QD with a fractional charge corresponding to $e^* = e/3$, as predicted theoretically. In the properly tuned regime, the tunnel coupling across the incompressible region is strong enough to enable tunneling of fractionally charged quasi-particles and weak enough to lead to a detectable Coulomb blockade signal via rearrangement of (fractional) charges. As each compressible region forms a QD, the quasi-particle tunneling can be treated in a capacitive single particle model as the fractional Coulomb blockade between two nested QDs. We construct a phase diagram of stable charge, which was previously proposed theoretically (*44*) and measured for integer Landau levels (*37*, *45*–*50*).

RESULTS AND DISCUSSION

Experimental setup and characterization

The QD sample is fabricated on an AlGaAs/GaAs heterostructure etched into a Hall bar structure. It hosts a two-dimensional electron gas (2DEG) 130 nm below the surface, which is contacted by annealed AuGeNi ohmic contacts. We measure a bulk electron density $n_{bulk} = 1.44 \times 10^{11}\text{cm}^{-2}$ and electron mobility $\mu = 5.6 \times 10^6\text{cm}^2/\text{Vs}$ at temperature $T = 30$ mK. The bulk electron density can be altered by applying a voltage to the prepatterned, overgrown back gate extending underneath the Hall bar 1 μm below the 2DEG (*51*). For all measurements in this paper, the back gate was grounded. However, the presence of back gates or additional gates can influence the confinement potential, which was exploited in previous experiments (*12*, *27*, *52*, *53*).

The detailed gate design of the inner structure of the QD sample is shown in Fig. 1A. The QD with a width of 1.4 μm and a lithographic area of $\approx 2\ \mu\text{m}^2$ is formed by four metallic gates [labeled center barrier (CB), left and right barriers (LB and RB), and plunger gate (PG); yellow] that are lithographically patterned on the surface of the AlGaAs/GaAs heterostructure (dark blue). We form the QD by applying negative voltages to the gates, thereby depleting the electron gas underneath. Depletion of the electron gas below the gate

[1]Solid State Physics Laboratory, Department of Physics, ETH Zurich, 8093 Zurich, Switzerland. [2]Institute for Theoretical Physics, Leipzig University Leipzig D-04009, Germany.
*Corresponding author. Email: marcro@phys.ethz.ch

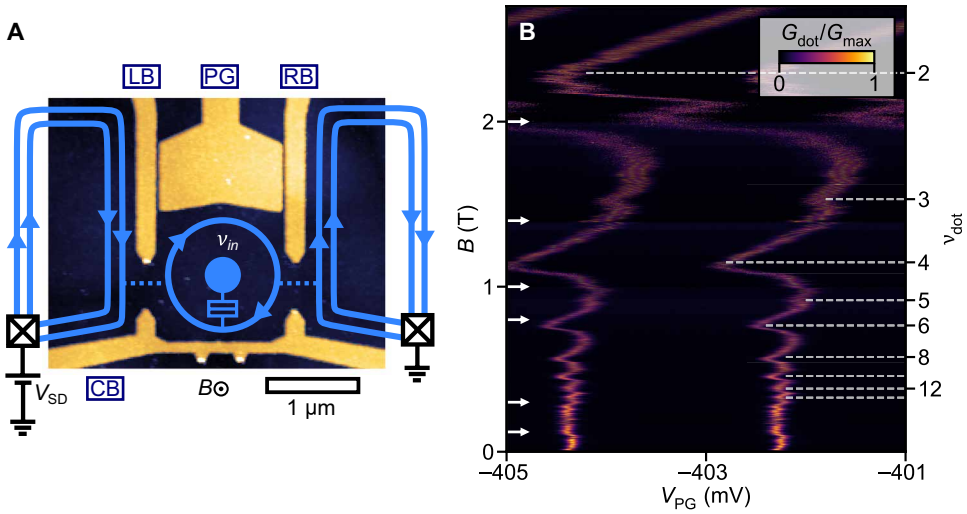

Fig. 1. Sample schematic and density characterization. (**A**) atomic force microscopy image of the QD device. Top gates (labeled LB, PG, RB, and CB) appear in yellow, while the uncovered semiconductor is dark blue. A magnetic field is applied perpendicular to the sample surface. The overlaid schematics show the chiral compressible regions separated by an incompressible $\nu_{in} = 1$ filling factor region for a bulk filling factor $\nu_b \approx 2$. We apply a source-drain bias V_{SD} and measure the current I_{SD}. (**B**) Normalized conductance G_{dot}/G_{max} through the QD as a function of the PG voltage V_{PG} and the magnetic field B, where G_{max} is the local maximum of the conductance over five adjacent PG voltage traces. Seven measurements with different barrier gate voltages V_{LB} and V_{RB} are combined by shifting in PG voltage such that the peaks match at the boundaries of the individual measurements. The boundaries between measurements are marked with white arrows. The Coulomb peaks show a $1/B$-periodic behavior that can be related to integer filling factors $\nu_{dot} = 2,3,4,5,6,8,10,12$, and 14 in the QD (dashed lines). Fitting these features results in an electron density $n_{dot} = (1.11 \pm 0.04) \times 10^{11}\text{cm}^{-2}$ in the QD. A corresponding filling factor (ν_{dot}) axis is indicated on the right.

occurs at −0.35 V. By applying a small voltage V_{SD} between the source and drain contacts and measuring the resulting current I_{SD}, we study the two-terminal linear conductance $G_{dot} = V_{SD}/I_{SD}$ of the QD. First, we tune the QD system into the Coulomb blockade regime. The CB gate and the LB and RB gates tune the transmission of the right and left barriers, respectively. The transmitted conductance through both barriers is set to $\ll e^2/h$ such that the QD is only weakly coupled to its leads. We fix the voltage of the CB gate $V_{CB} = -1.2$ V, while the voltage on LB and RB is changed to retune the barrier coupling of the QD for different measurements. The voltage on the PG is varied around $V_{PG} \approx -0.4$ V and used to tune the discrete energy levels of the QD.

The measurements were conducted in a dilution refrigerator at the base temperature $T = 30$ mK. All measurements presented within this paper were performed on the same sample during one cooldown. The presented modulation of the Coulomb peaks was reproduced in a second cooldown with similar gate voltages. In addition, similar measurements were reproduced with another sample using a different heterostructure and gate design.

The electron density in the QD region is reduced compared to the bulk density of the 2DEG by the applied confining gate voltages. To estimate the effective electron density n_{dot} inside the QD, we analyze the conductance G_{dot} through the QD in the integer quantum Hall regime. Figure 1B shows the normalized conductance G_{dot}/G_{max} as a function of magnetic field B applied perpendicular to the sample surface and the PG voltage V_{PG}. For improved visibility of all resonances, each conductance trace (PG voltage varied, magnetic field fixed) is normalized by the maximal local conductance G_{max} of the five adjacent traces. In addition, the transmission of the barriers of the QD changes slowly with magnetic field. Therefore, the barrier gate voltages V_{LB} and V_{RB} needed to be retuned at some magnetic fields to ensure that the conductance through the barriers stays in the desired range of weak coupling. In Fig. 1B, we therefore combine seven measurements taken over finite magnetic field ranges where different barrier gate voltage settings were applied (transitions marked by arrows). We combine the seven measurements into one figure by shifting them in PG voltage such that the peaks match at the boundary of the individual measurements. We observe Coulomb blockade resonances as a function of the PG voltage. Their position in gate voltage shows a $1/B$-periodic modulation as indicated by dashed lines in Fig. 1B. This $1/B$-periodic oscillation is directly related to the changing quantum capacitance of the QD that follows the $1/B$-dependent density of states at the Fermi energy. Identifying these features with integer filling factors $\nu_{dot} = 2,3,4,5,6,8,10,12$, and 14 in the QD allows us to extract the electron density $n_{dot} = (1.11 \pm 0.04) \times 10^{11}\text{cm}^{-2}$ in the QD by fitting the relation $\nu = n_{dot}h/(eB)$. All of the 1/B-periodic modulations used for determining the density n_{dot} in the QD are within the magnetic field range of one single measurement with one specific gate voltage setting. We will see later that this density corresponds to the maximum local density in the QD center.

Periodic modulation of Coulomb resonances for fractional filling

We now study the conductance of the weakly coupled QD in the fractional quantum Hall regime for filling factor $\nu_{dot} \gtrsim 2/3$ and compare it to the integer quantum Hall regime at $\nu_{dot} \approx 2$. First, we look at the conductance around filling factor $\nu_{dot} \approx 2$ as a function of PG voltage and magnetic field shown in Fig. 2A. The Coulomb resonances show a distinct periodic pattern in magnetic field that has been studied in previous works (*36*, *37*, *47*, *49*, *50*). The pattern originates from an interplay of the two compressible regions emerging from the two filled Landau levels at filling factor 2 as schematically depicted by the light blue regions in Fig. 1A. Regions of

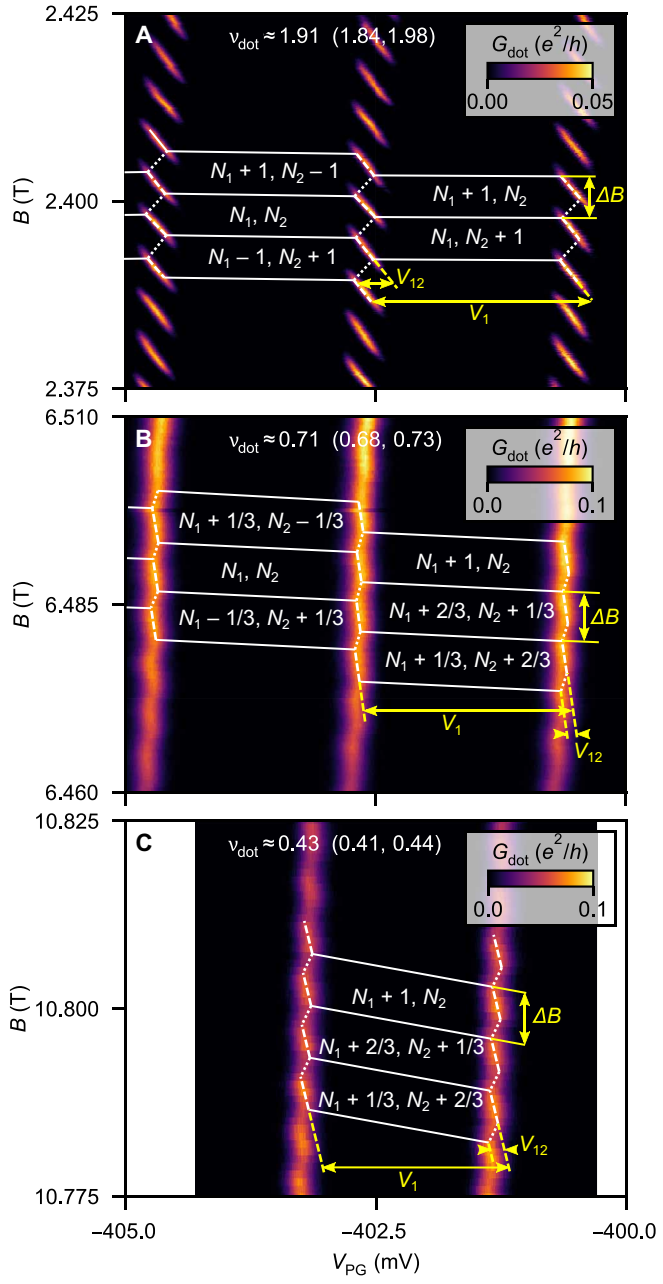

Fig. 2. Conductance G_{dot} as a function of the PG voltage V_{PG} and the magnetic field B for different dot filling factors. (**A**) $\nu_{dot} \approx 2$, (**B**) $\nu_{dot} \gtrsim 2/3$, and (**C**) $\nu_{dot} \gtrsim 1/3$. The exact dot filling factor ν_{dot} at the middle of the magnetic field range is indicated with experimental uncertainty in parentheses. Regions of constant charge (N_1, N_2) are indicated in the charge stability diagram by white lines. The charge on the outer and inner compressible regions is denoted by eN_1 and eN_2, respectively. The situation for and 1/3 in (B) and (C) allows for fractional charging of $e^* = e/3$.

stable charge (N_1 and N_2) (separated by white lines in Fig. 2A) can be described by a capacitance model (*33*, *35*, *37*, *44*) where N_1 and N_2 correspond to the number of electrons on the outer and inner compressible region, respectively.

Changing to the fractional quantum Hall regime, the conductance depending on the magnetic field and the PG voltage is shown in Fig. 2B around filling factor $\nu_{dot} \gtrsim 2/3$. The Coulomb resonances of the QD show a periodic modulation in the amplitude and the position in PG voltage as a function of the magnetic field. The modulations are clearly visible while being less pronounced and extended compared to filling factor 2. The visible conductance resonances are continuously connected, in contrast to the clearly separated resonances around filling factor 2. The observation of modulated Coulomb resonances suggests the existence of a nontrivial fractional quantum Hall state inside the QD. Such a periodic pattern has previously not been observed for QDs in the fractional quantum Hall regime for filling factor $\nu_{dot} < 1$ to the best of our knowledge.

To further study the modulated Coulomb oscillations at filling factor $\nu_{dot} \gtrsim 2/3$ and get quantitative predictions, we extend the model for the integer quantum Hall effect discussed in our previous work (*37*) to fractional filling factors. We assume the existence of two compressible regions for the fractional filling factor $\nu_{dot} \gtrsim 2/3$ separated by an incompressible $\nu_{in} = 2/3$ region as schematically depicted in Fig. 1A and similar to the situation at $\nu_{dot} = 2$ where the incompressible region assumes filling factor $\nu_{in} = 1$. In thermodynamic equilibrium, the charge distribution in the QD minimizes the electrostatic energy. Changing the magnetic field by δB or the PG voltage by δV_{PG} charge imbalances δQ_i ($i = 1,2$) arise between the outer ($i = 1$) and inner ($i = 2$) compressible region

$$\begin{aligned} \delta Q_1 &= \Delta n_1 - \nu_{in}\delta B\bar{A}/\phi_0 - C_1\delta V_{PG}/e \\ \delta Q_2 &= \Delta n_2 + \nu_{in}\delta B\bar{A}/\phi_0 - C_2\delta V_{PG}/e \end{aligned} \quad (1)$$

The charge imbalances δQ_i are denoted in units of the elementary charge e. The Δn_i describes discrete changes in charge of the respective region due to quasi-particle tunneling to the other compressible region or the leads. In the fractional quantum Hall regime, this can take fractional values corresponding to a multiple of the fractional charge e^* for tunneling events between the compressible regions and is not required to be an integer number of the elementary charge e. Changing the magnetic flux through the area $\bar{A}$ enclosed by the incompressible stripe at $\nu_{in} = 2/3$, a Hall current $\nu_{in}\delta B\bar{A}/\phi_0$ will flow from the outer to the inner compressible region. Consequently, the (fractional) charge $\nu_{in}e$ will be shifted when adding one flux quantum $\phi_0 = h/e$, not necessarily corresponding to the quasi-particle charge e^*. The PG couples to the compressible regions over the effective capacitances $C_i > 0$. The change in total electrostatic energy can then be calculated to be

$$\delta E = \frac{1}{2}K_1\delta Q_1^2 + \frac{1}{2}K_2\delta Q_2^2 + K_{12}\delta Q_1\delta Q_2 \quad (2)$$

where the K_i ($i = 1,2$) describes the charging energies of the compressible regions and K_{12} the cross-charging energy due to capacitive coupling between the compressible regions. This model predicts hexagonally shaped regions of stable charge as a function of the magnetic field and PG voltage as the system minimizes the energy functional (Eq. 2) by assuming suitable Δn_i.

We interpret the data in Fig. 2B at $\nu_{dot} \gtrsim 2/3$ according to this model and draw the charge stability diagram. We will now look at charging events where a fractional charge e^* is rearranged between the two compressible regions, i.e., $\Delta n_1 = +e^*/e$, $\Delta n_2 = -e^*/e$. The corresponding magnetic field spacing ΔB coincides with the magnetic field period as indicated in Fig. 2B. The measured magnetic field period ΔB is shown in Fig. 3A as a function of magnetic field B for the regions where periodic modulations are observed. We find a

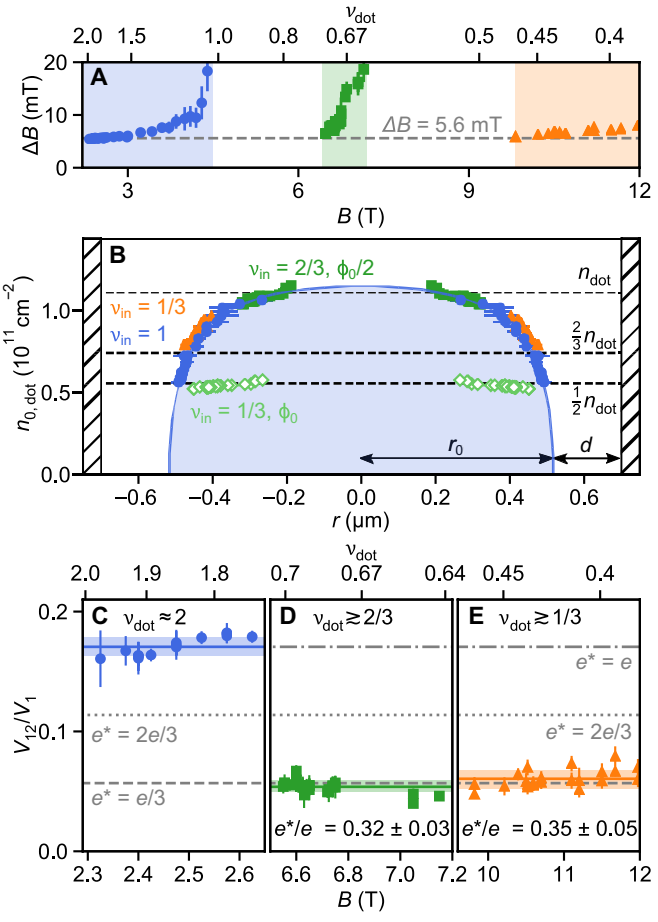

Fig. 3. Analysis of periodicity in magnetic field and gate voltage. (**A**) Magnetic field period ΔB indicated in Fig. 2 (A to C) as a function of magnetic field B. A periodic modulation is only observed for the shaded magnetic field regions. (**B**) Zero magnetic field density $n_{0,\,dot}$ of the QD as a function of the radius r calculated from the magnetic field periodicities in (A) according to Eqs. 3 and 4, mirrored around $r = 0$. We assume a magnetic field periodicity ΔB corresponding to a flux quantum ϕ_0 for $2 > \nu_{dot} > 1$ [(C), blue dots] and $\nu_{dot} \gtrsim 1/3$ [(E), orange triangles] and $\phi_0/2$ for $\nu_{dot} \gtrsim 2/3$ [(D), green squares]. Assuming a flux quantum periodicity ϕ_0 and an incompressible stripe at $\nu_{in} = 1/3$ for $\nu_{dot} \gtrsim 2/3$ instead (light green empty diamonds), the calculated charge distribution does not agree with the data of other filling factors. The blue line shows a fit according to Eq. 5. (**C** to **E**) Ratio V_{12}/V_1 of the PG voltages indicated in Fig. 2 (A and B) depending on B for dot filling factors around (C) $\nu_{dot} \approx 2$, (D) $\nu_{dot} \gtrsim 2/3$, and (E) $1/2 > \nu_{dot} \gtrsim 1/3$. Quasi-particle charge ratios e^*/e calculated by Eq. 8 are indicated.

stable period of $\Delta B = 5.6$ mT (corresponding to an area $\bar{A} = 0.74\,\mu m^2$) at $\nu_{dot} \approx 2$ (blue dots) slowly rising toward and diverging at $\nu_{dot} \approx 1$, which is directly related to the decreasing area enclosed by the incompressible $\nu_{in} = 1$ stripe as the upper spin-split branch of the lowest Landau level is depopulated (*37*). For $\nu_{dot} \gtrsim 2/3$ (green squares), the period quickly increases with increasing B as well.

Periodic modulations of the conductance are also observed for filling factors $1/2 > \nu_{dot} > 1/3$ as shown in Fig. 2C as a function of PG voltage and magnetic field (see also Fig. 4, G and H). The charge stability diagram is indicated and very similar to $\nu_{dot} \gtrsim 2/3$ in Fig. 2B. For the region where $\nu_{dot} \gtrsim 1/3$, the QD exhibits two compressible regions separated by an incompressible region at $\nu_{in} = 1/3$, and we can apply the same model as described above for $\nu_{dot} \gtrsim 2/3$ where $\nu_{in} = 2/3$. The corresponding magnetic period for $1/2 > \nu_{dot} > 1/3$ is displayed in Fig. 3A (orange triangles) and shows a slow increase similar to the behavior close to $\nu_{dot} \approx 2$. For all three regimes ($\nu_{in} = 1$, 2/3, or 1/3) in Fig. 3A, a periodic modulation is only observed for $\nu_{dot} \gtrsim \nu_{in}$ within the experimental uncertainty that stems from the uncertainty in the calculated dot density n_{dot}.

Extracting the dot density distribution

The magnetic field spacing between two rearrangements resulting from the model is $\Delta B = (e^*/e)\,\phi_0/(\nu_{in}\bar{A})$. Assuming a circular charge distribution of the QD, we can calculate the radius of the incompressible region according to

$$r(B) = \sqrt{\frac{e^*/e}{\nu_{in}}\frac{\phi_0}{\Delta B \pi}} \tag{3}$$

with a density in the incompressible region

$$n(r, B) = \frac{eB}{h}\nu_{in} \tag{4}$$

Using these two equations enables us to reconstruct the zero magnetic field charge density distribution $n_{0,\,dot}$ in the QD from the measured magnetic period $\Delta B(B)$ in Fig. 3A. We assume fractional charge $e^* = e/3$ for $\nu_{dot} \gtrsim 1/3$ and 2/3 and charge e for $\nu_{dot} \approx 2$ while having an incompressible region at $\nu_{in} = 1/3$, 2/3, and 1, respectively. This results in the dot density $n_{0,dot}$ shown in Fig. 3B with a flux quantum periodicity ϕ_0 for $\nu_{dot} \approx 2$ (blue dots) and $\nu_{dot} \gtrsim 1/3$ (orange triangles) and a half-flux quantum periodicity $\phi_0/2$ for $\nu_{dot} \gtrsim 2/3$ (green squares). All three different regimes line up to form a smooth radial density dependence. The slightly higher radii for $\nu_{dot} \gtrsim 1/3$ probably reflect the lower voltages applied to the barrier gates in this regime. For $\nu_{dot} \gtrsim 2/3$, we can exclude periodic modulations spaced by a full flux quantum ϕ_0 that would originate from an incompressible region of $\nu_{in} = 1/3$. They would lead to the light green, empty diamonds in Fig. 3B that do not line up with the points of the other regimes.

In a study of an anti-dot embedded into a $\nu = 2/3$ fractional quantum Hall (FQH) state (*9*), a flux period of ϕ_0 was found. This experiment was analyzed with the help of an electrostatic model which assumed that the edge of the $\nu = 2/3$ quantum Hall state consists of a downstream propagating integer channel and an upstream propagating fractional 1/3 channel (*54*). This edge structure was proposed by MacDonald (*55*). Depending on the strength of the Coulomb repulsion between these channels, the flux periodicity was found to be ϕ_0 for weak coupling and $\phi_0/2$ for strong coupling. In the latter case, the two channels can be described as a single compressible region, as in our model. In the present experiment, we cannot distinguish any additional ϕ_0 period. We conclude that in our experiment the 2/3 edge does not exhibit signatures of an additional neutral mode. The absence of other incompressible stripes with fractional filling factors <2/3 might be due to the increasing steepness of the confining potential closer to the edge. Edge reconstruction will only occur when the fractional gap exceeds the potential gradient times the magnetic length.

We can fit the dot density $n_{0,dot}(r)$ in Fig. 3B using a model proposed by Lier and Gerhardts (*56*) for the position of incompressible stripes at the gated edge of quantum Hall systems. The presence of a charged gate leads to a reduction of the bulk density n_{bulk} by a

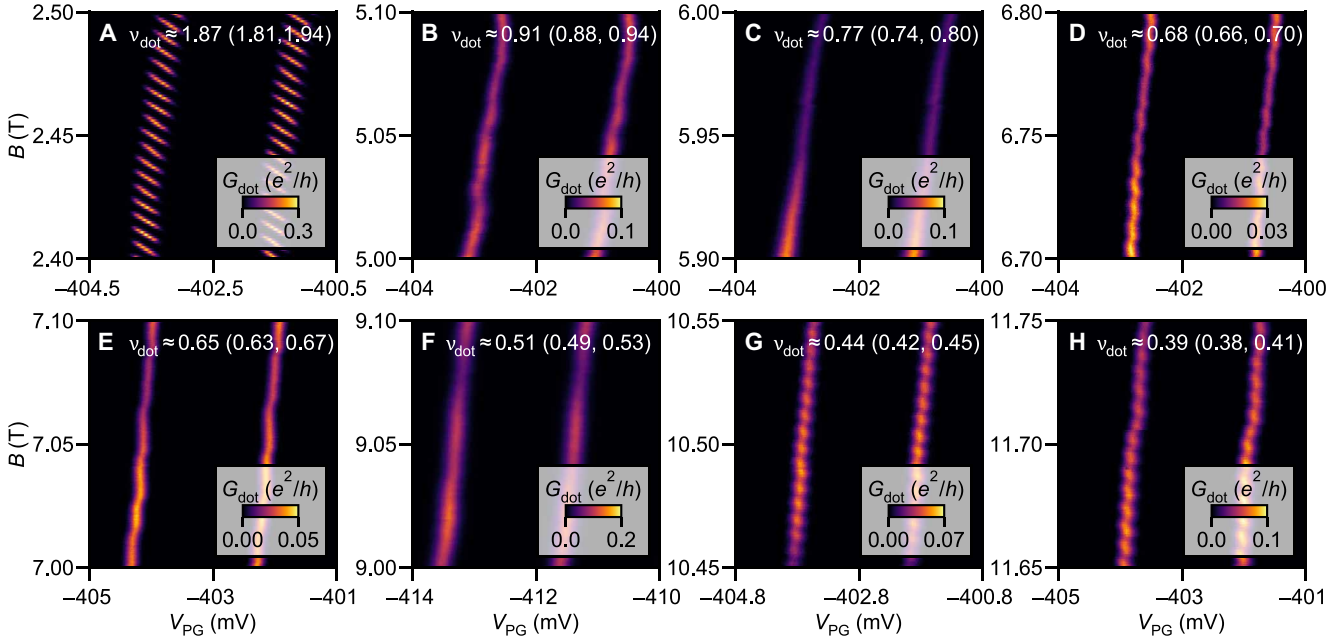

Fig. 4. Conductance G_{dot} as a function of the PG voltage V_{PG} and the magnetic field B for decreasing dot filling factors $2>\nu_{dot}>1/3$. The filling factor ν_{dot} is indicated with the corresponding experimental uncertainty in parentheses. Periodic modulation of the Coulomb peaks are observed in (**A**), (**D**), (**E**), (**G**), and (**H**) corresponding to filling factors in the regions marked in Fig. 3A. No periodic modulations are observed in (**B**), (**C**), and (**F**).

factor s. To calculate the density distribution, we assume two gates placed symmetrically around the center at $r = 0$ resulting in

$$n_{0,\mathrm{dot}}(r) = n_{\mathrm{bulk}}\, s(r, r_0, d)\, s(r, -r_0, -d) \text{ with}$$
$$s(r, r_0, d) = \sqrt{(r_0 - r)/(r_0 + d - r)} \tag{5}$$

where r_0 is the radius where the density drops to 0 and d is the depletion length around the gate. The fit (blue line) to our data at $\nu_{dot} \approx 2$ is shown in Fig. 3B with $r_0 = (517 \pm 1)$nm and $d = (131 \pm 4)$ nm. This agrees well with the lithographic dot size $r_{lith} \approx 0.7\,\mu\mathrm{m} \approx r_0 + d$.

From electrostatic simulations using COMSOL, we calculate a magnetic field period $\Delta B = 6.3$ mT at a magnetic field of $B = 10$T for filling factor $\nu_{dot} \gtrsim 1/3$ and gate voltages comparable to the experimentally applied values, which is in good agreement with the experimentally determined value. Similarly, we get $\Delta B = 11.6$ mT at a magnetic field of $B = 7$T for filling factor $\nu_{dot} \gtrsim 2/3$, again in good agreement with the experiment. The calculated total charge on the QD corresponds roughly to $N_{tot}^{(sim)} = 870$ electrons. This is comparable to the experimentally derived value of $N_{tot}^{(exp)} = 820$ from experimental values for the density n_{dot} and the area $\bar{A}$. The results of the electrostatic simulations agree well with the experimental observations.

Returning to the charge stability diagram in Fig. 2B, we calculate within our model the slope of an internal charging line between the two compressible regions

$$\left.\frac{\delta B}{\delta V_{PG}}\right|_{rearr.} = -\frac{1}{\nu_{in}} \frac{\phi_0 e(\alpha_1 - \alpha_2)}{\bar{A}\,[(K_1 - K_{12}) + (K_2 - K_{12})]} < 0 \tag{6}$$

where $\alpha_1 = (K_1C_1 + K_{12}C_2)/e^2$ and $\alpha_2 = (K_{12}C_1 + K_2C_2)/e^2$ denote the lever arms of the PG on the respective compressible region. This slope is negative as generally $\alpha_1 > \alpha_2$, which limits the ways we can draw the recharging lines connecting the visible Coulomb oscillations. In addition, we calculate the slopes corresponding to a constant charge on either of the two compressible regions

$$\left.\frac{\delta B}{\delta V_{PG}}\right|_{\Delta n_1 = 0} = -\frac{1}{\nu_{in}} C_1 \phi_0/(e\bar{A}) < 0,$$
$$\left.\frac{\delta B}{\delta V_{PG}}\right|_{\Delta n_2 = 0} = \frac{1}{\nu_{in}} C_2 \phi_0/(e\bar{A}) > 0 \tag{7}$$

These constraints define the orientation of hexagons in the charge stability diagram as shown in Fig. 2B. Crossing any segment of the hexagon boundary with nonzero conductance in V_{PG} direction in Fig. 2B, the total charge on the QD changes by e. We see that crossing the boundary segment with negative slope implies $\Delta n_1 = 1$ and $\Delta n_2 = 0$, while crossing it along a segment with positive slope corresponds to $\Delta n_1 = 2/3$ and $\Delta n_2 = 1/3$. The charge of an electron tunneling into the QD can therefore be split among the compressible regions into fractional quasi-particle charges. This could be the reason why the Coulomb resonances are connected for $\nu_{dot} \lesssim 2/3$ (Fig. 2B). At $\nu_{dot} \approx 2$, on the other hand, the Corbino $\gtrsim$conductance across the incompressible region might be very small, such that electron tunneling into the inner compressible region is not substantial on transport time scales, giving rise to clearly separated resonances (Fig. 2A).

Fractional charge

So far, we have considered ideal values for the fractional charge to determine the flux periodicities, the density distribution, and the parameter of the charging model. Now, we extract an experimental value for the quasi-particle charge for fractional filling factors $\nu_{dot} \gtrsim 2/3$ and 1/3 by further analyzing the charge stability diagram for the integer and fractional quantum Hall regimes in Fig. 2. To this end, we calculate from the model the voltage differences $V_1 = K_1/(e\alpha_1)$ and $V_{12} = (e^*/e)(K_1 - K_{12})/(e\alpha_1)$, which appear in the measurements

in Fig. 2 (A to C) as separations of visible charging lines as indicated. By taking the ratio V_{12}/V_1, we eliminate the lever arm α_1. Assuming that the ratio K_1/K_{12} is independent of the filling factor, the quasi-particle charge is then calculated by comparing the ratios for the integer and fractional filling factors

$$\frac{e^*}{e} = \frac{V_{12}^{(\mathrm{fract})}/V_1^{(\mathrm{fract})}}{V_{12}^{(\mathrm{int})}/V_1^{(\mathrm{int})}} \quad (8)$$

Figure 3 (C to E) shows the ratio V_{12}/V_1 as a function of the magnetic field for filling factors around $\nu_{dot} \approx 2$, $\gtrsim 2/3$, and $\gtrsim 1/3$. Each point corresponds to a measurement as depicted in Fig. 2 (A to C) centered around a certain magnetic field value. The extracted relevant parameters are averaged over several hexagons of such a charge stability diagram. The ratio V_{12}/V_1 is roughly constant within each filling factor regime. We extract a fractional charge $e^*/e = 0.32 \pm 0.03$ and $e^*/e = 0.35 \pm 0.05$, respectively, by comparison to $\nu_{dot} \approx 2$. This indicates a fractional charge $e^* = e/3$ for quasi-particles tunneling in the QD for both $\nu_{dot} \gtrsim 2/3$ and $\gtrsim 1/3$. For $\nu = 1/3$, fractional charge $e^* = e/3$ has previously been found from measurements on shot noise (*3*, *4*), localized states (*8*), photo-assisted shot noise (*10*), or quantum Hall Fabry-Pérot interferometers (*12*), while at $\nu = 2/3$, different experiments indicated different values, namely, $e/3$ (*7*, *11*), $2e/3$ (*7*, *9*), and e (*12*).

Evolution for different filling factors

To give an overview of the evolution of the conductance measurements for decreasing filling factors $2 > \nu_{dot} > 1/3$, we show additional data in Fig. 4. As indicated in Fig. 3A, periodic modulations of the Coulomb resonances are only observed within the marked regions. The evolution from the distinct pattern at $\nu_{dot} = 2$ in Fig. 4A toward filling factor 1 has been studied in detail in previous work (*37*) and is found here to behave in the same way. For a regime $1 > \nu_{dot} \gtrsim 0.75$, the Coulomb resonances show no periodic modulations as seen in Fig. 4 (B and C). In the fractional quantum Hall regime, the Coulomb resonances are modulated around filling factor $\nu_{dot} \gtrsim 2/3$ and $1/2 > \nu_{dot}$ as shown in Fig. 4 (D, E, G, and H). The two regions are interrupted by a region around filling factor $\nu_{dot} = 1/2$ where no modulations are observed (see Fig. 4F).

Conclusion

In conclusion, we have studied the magneto-conductance of a 1.4-μm-wide QD in the fractional quantum Hall regime for filling factors $\nu < 1$. Around $\nu_{dot} \gtrsim 2/3$ and $1/2 > \nu_{dot} > 1/3$, we observe periodic modulations of Coulomb resonances as a function of magnetic field. Assuming two compressible regions separated by an incompressible stripe at $\nu_{in} = 2/3$ and $\nu_{in} = 1/3$, respectively, we have successfully used an electrostatic model to describe the phase diagram as a function of magnetic field and PG voltage. We extract the charge density distribution of the QD at zero magnetic field. By comparing our measurements in the fractional regime with measurements at $\nu_{dot} \approx 2$, we find fractional Coulomb blockade between the compressible regions in the QD with quasi-particle tunneling of fractional charge $e^*/e = 0.32 \pm 0.03$ and $e^*/e = 0.35 \pm 0.05$ for the two fractional regimes, respectively. QDs and quantum Hall Fabry-Pérot interferometers have been shown to be closely related in the integer quantum Hall regime (*33*–*37*). We have demonstrated experimentally that this relation persists in the fractional regime. Groundbreaking recent experiments have detected anyonic phase jumps in a Fabry-Pérot interferometer at fractional filling 1/3 (*29*), and fractional anyonic statistics were observed in anyon collision experiments (*28*). While interferometry experiments in the fractional quantum Hall regime have been shown to be very intricate and sensitive (*1*, *12*, *18*, *27*, *29*), fully Coulomb blockaded devices may provide an alternative experimental approach. Our observations complement and extend interferometry experiments of fractional quantum Hall states.

MATERIALS AND METHODS

Sample fabrication

The sample is fabricated using standard semiconductor fabrication techniques. We use a wafer that is overgrown with a standard modulation doped single interface AlGaAs/GaAs heterostructure by the Wegscheider group. The interface where the 2DEG accumulates lies 130 nm below the surface. The Si δ-doping layer lies 60 nm below the surface with a spacer of 70 nm to the 2DEG. A patterned back gate is added before overgrowth in an established process detailed in (*51*) and lies roughly 1 μm below the 2DEG. The mesa is patterned using optical lithography and wet etched with diluted Piranha acid (H_2O:H_2O_2:H_2SO_4, 100:3:3) with an etching depth slightly deeper than the 2DEG. Ohmic contacts are patterned using optical lithography. Using electron beam evaporation, we deposit a eutectic mixture of Ge/Au/Ni onto the sample and anneal at 500°C for 300 s [in 200 sccm H_2/N_2 (5%) flow] after liftoff. Then, we pattern the bond pads and large gate leads with optical lithography and evaporate a Ti/Au (10 nm/80 nm) layer. The small gate structures that form the QD are patterned using electron beam lithography. The gates are then deposited by electron beam evaporation of Ti/Au (5 nm/25 nm). We check the gate structure with atomic force microscopy lithography (see Fig. 1A).

Measurement techniques

The sample is cooled down in a wet dilution refrigerator at a base temperature $T = 30$ mK. All lines connected to the sample are filtered with a cold lowpass RC filter ($R = 10$ kΩ, $C = 1$ nF, $f_{cutoff} \approx 15$ kHz or $R = 1$ kΩ, $C = 100$ pF, $f_{cutoff} \approx 1.5$ MHz) at the cold finger. The current I_{SD} through the sample is measured by applying a voltage bias V_{SD} over an current to voltage converter to the sample contact and measuring the resulting voltage over the reference resistance. The conductance is calculated as the ratio $G_{dot} = I_{SD}/V_{SD}$. The IV converter is temperature stabilized, and offset voltages are corrected for.

SUPPLEMENTARY MATERIALS

Supplementary material for this article is available at http://advances.sciencemag.org/cgi/content/full/7/19/eabf5547/DC1

REFERENCES AND NOTES

1. R. Sabo, I. Gurman, A. Rosenblatt, F. Lafont, D. Banitt, J. Park, M. Heiblum, Y. Gefen, V. Umansky, D. Mahalu, Edge reconstruction in fractional quantum Hall states. *Nat. Phys.* **13**, 491–496 (2017).
2. A. M. Chang, Chiral Luttinger liquids at the fractional quantum Hall edge. *Rev. Mod. Phys.* **75**, 1449–1505 (2003).
3. R. de Picciotto, M. Reznikov, M. Heiblum, V. Umansky, G. Bunin, D. Mahalu, Direct observation of a fractional charge. *Nature* **389**, 162–164 (1997).
4. L. Saminadayar, D. C. Glattli, Y. Jin, B. Etienne, Observation of the e/3 fractionally charged Laughlin quasiparticle. *Phys. Rev. Lett.* **79**, 2526–2529 (1997).
5. M. Reznikov, R. de Picciotto, T. G. Griffiths, M. Heiblum, V. Umansky, Observation of quasiparticles with one-fifth of an electron's charge. *Nature* **399**, 238–241 (1999).
6. M. Dolev, M. Heiblum, V. Umansky, A. Stern, D. Mahalu, Observation of a quarter of an electron charge at the ν = 5/2 quantum Hall state. *Nature* **452**, 829–834 (2008).

7. A. Bid, N. Ofek, M. Heiblum, V. Umansky, D. Mahalu, Shot noise and charge at the 2/3 composite fractional quantum Hall state. *Phys. Rev. Lett.* **103**, 236802 (2009).
8. J. Martin, S. Ilani, B. Verdene, J. Smet, V. Umansky, D. Mahalu, D. Schuh, G. Abstreiter, A. Yacoby, Localization of fractionally charged quasi-particles. *Science* **305**, 980–983 (2004).
9. A. Kou, C. M. Marcus, L. N. Pfeiffer, K. W. West, Coulomb oscillations in antidots in the integer and fractional quantum Hall regimes. *Phys. Rev. Lett.* **108**, 256803 (2012).
10. M. Kapfer, P. Roulleau, M. Santin, I. Farrer, D. A. Ritchie, D. C. Glattli, A Josephson relation for fractionally charged anyons. *Science* **363**, 846–849 (2019).
11. R. Bisognin, H. Bartolomei, M. Kumar, I. Safi, J.-M. Berroir, E. Bocquillon, B. Placais, A. Cavanna, U. Gennser, Y. Jin, G. Fève, Microwave photons emitted by fractionally charged quasiparticles. *Nat. Commun.* **10**, 1708 (2019).
12. J. Nakamura, S. Fallahi, H. Sahasrabudhe, R. Rahman, S. Liang, G. C. Gardner, M. J. Manfra, Aharonov-Bohm interference of fractional quantum Hall edge modes. *Nat. Phys.* **15**, 563–569 (2019).
13. B. J. van Wees, L. P. Kouwenhoven, C. J. P. M. Harmans, J. G. Williamson, C. E. Timmering, M. E. I. Broekaart, C. T. Foxon, J. J. Harris, Observation of zero-dimensional states in a one-dimensional electron interferometer. *Phys. Rev. Lett.* **62**, 2523–2526 (1989).
14. R. P. Taylor, A. S. Sachrajda, P. Zawadzki, P. T. Coleridge, J. A. Adams, Aharonov-Bohm oscillations in the Coulomb blockade regime. *Phys. Rev. Lett.* **69**, 1989–1992 (1992).
15. J. P. Bird, K. Ishibashi, Y. Aoyagi, T. Sugano, Precise period doubling of the Aharonov-Bohm effect in a quantum dot at high magnetic fields. *Phys. Rev. B* **53**, 3642–3645 (1996).
16. M. D. Godfrey, P. Jiang, W. Kang, S. H. Simon, K. W. Baldwin, L. N. Pfeiffer, K. W. *West, Aharonov-Bohm-Like Oscillations in Quantum Hall Corrals* (2007); arXiv:0708.2448.
17. F. E. Camino, W. Zhou, V. J. Goldman, Aharonov-Bohm electron interferometer in the integer quantum Hall regime. *Phys. Rev. B* **72**, 155313 (2005).
18. N. Ofek, A. Bid, M. Heiblum, A. Stern, V. Umansky, D. Mahalu, Role of interactions in an electronic Fabry-Perot interferometer operating in the quantum Hall effect regime. *Proc. Natl. Acad. Sci. U.S.A.* **107**, 5276–5281 (2010).
19. F. E. Camino, W. Zhou, V. J. Goldman, Aharonov-Bohm superperiod in a Laughlin quasiparticle interferometer. *Phys. Rev. Lett.* **95**, 246802 (2005).
20. W. Zhou, F. E. Camino, V. J. Goldman, Flux-period scaling in the Laughlin quasiparticle interferometer. *Phys. Rev. B* **73**, 245322 (2006).
21. F. E. Camino, W. Zhou, V. J. Goldman, e/3 Laughlin quasiparticle primary-filling $\nu = 1/3$ interferometer. *Phys. Rev. Lett.* **98**, 076805 (2007).
22. F. E. Camino, W. Zhou, V. J. Goldman, Quantum transport in electron Fabry-Perot interferometers. *Phys. Rev. B* **76**, 155305 (2007).
23. P. V. Lin, F. E. Camino, V. J. Goldman, Electron interferometry in the quantum Hall regime: Aharonov-Bohm effect of interacting electrons. *Phys. Rev. B* **80**, 125310 (2009).
24. D. T. McClure, W. Chang, C. M. Marcus, L. N. Pfeiffer, K. W. West, Fabry-Perot interferometry with fractional charges. *Phys. Rev. Lett.* **108**, 256804 (2012).
25. R. L. Willett, L. N. Pfeiffer, K. W. West, Measurement of filling factor 5/2 quasiparticle interference with observation of charge e/4 and e/2 period oscillations. *Proc. Natl. Acad. Sci. U.S.A.* **106**, 8853–8858 (2009).
26. R. L. Willett, L. N. Pfeiffer, K. W. West, Alternation and interchange of e/4 and e/2 period interference oscillations consistent with filling factor 5/2 non-Abelian quasiparticles. *Phys. Rev. B* **82**, 205301 (2010).
27. R. L. Willett, K. Shtengel, C. Nayak, L. N. Pfeiffer, Y. J. Chung, M. L. Peabody, K. W. Baldwin, K. W. West, *Interference Measurements of Non-Abelian e/4 & Abelian e/2 Quasiparticle Braiding* (2019); arXiv:1905.10248.
28. H. Bartolomei, M. Kumar, R. Bisognin, A. Marguerite, J.-M. Berroir, E. Bocquillon, B. Plaçais, A. Cavanna, Q. Dong, U. Gennser, Y. Jin, G. Fève, Fractional statistics in Anyon collisions. *Science* **368**, 173–177 (2020).
29. J. Nakamura, S. Liang, G. C. Gardner, M. J. Manfra, Direct observation of anyonic braiding statistics. *Nat. Phys.* **16**, 931–936 (2020).
30. Y. Ji, Y. Chung, D. Sprinzak, M. Heiblum, D. Mahalu, H. Shtrikman, An electronic Mach-Zehnder interferometer. *Nature* **422**, 415–418 (2003).
31. K. T. Law, D. E. Feldman, Y. Gefen, Electronic Mach-Zehnder interferometer as a tool to probe fractional statistics. *Phys. Rev. B* **74**, 045319 (2006).
32. D. E. Feldman, A. Kitaev, Detecting non-Abelian statistics with an electronic Mach-Zehnder interferometer. *Phys. Rev. Lett.* **97**, 186803 (2006).
33. B. Rosenow, B. I. Halperin, Influence of interactions on flux and back-gate period of quantum Hall interferometers. *Phys. Rev. Lett.* **98**, 106801 (2007).
34. A. Stern, B. Rosenow, R. Ilan, B. I. Halperin, Interference, Coulomb blockade, and the identification of non-Abelian quantum Hall states. *Phys. Rev. B* **82**, 085321 (2010).
35. B. I. Halperin, A. Stern, I. Neder, B. Rosenow, Theory of the Fabry-Pérot quantum Hall interferometer. *Phys. Rev. B* **83**, 155440 (2011).
36. I. Sivan, H. K. Choi, J. Park, A. Rosenblatt, Y. Gefen, D. Mahalu, V. Umansky, Observation of interaction-induced modulations of a quantum Hall liquid's area. *Nat. Commun.* **7**, 12184 (2016).
37. M. P. Rössli, L. Brem, B. Kratochwil, G. Nicolí, B. A. Braem, S. Hennel, P. Märki, M. Berl, C. Reichl, W. Wegscheider, K. Ensslin, T. Ihn, B. Rosenow, Observation of quantum Hall interferometer phase jumps due to a change in the number of bulk quasiparticles. *Phys. Rev. B* **101**, 125302 (2020).
38. D. B. Chklovskii, B. I. Shklovskii, L. I. Glazman, Electrostatics of edge channels. *Phys. Rev. B* **46**, 4026–4034 (1992).
39. R. J. Brown, C. G. Smith, M. Pepper, M. J. Kelly, R. Newbury, H. Ahmed, D. G. Hasko, J. E. F. Frost, D. C. Peacock, D. A. Ritchie, G. A. C. Jones, Resonant magneto-transport through a lateral quantum box in a semiconductor heterostructure. *J. Phys. Condens. Matter* **1**, 6291–6298 (1989).
40. P. L. McEuen, E. B. Foxman, U. Meirav, M. A. Kastner, Y. Meir, N. S. Wingreen, S. J. Wind, Transport spectroscopy of a Coulomb island in the quantum Hall regime. *Phys. Rev. Lett.* **66**, 1926–1929 (1991).
41. P. L. McEuen, E. B. Foxman, J. Kinaret, U. Meirav, M. A. Kastner, N. S. Wingreen, S. J. Wind, Self-consistent addition spectrum of a Coulomb island in the quantum Hall regime. *Phys. Rev. B* **45**, 11419–11422 (1992).
42. P. L. McEuen, N. S. Wingreen, E. B. Foxman, J. Kinaret, U. Meirav, M. A. Kastner, Y. Meir, S. J. Wind, Coulomb interactions and energy-level spectrum of a small electron gas. *Phys. B Condens. Matter* **189**, 70–79 (1993).
43. J. Dempsey, B. Y. Gelfand, B. I. Halperin, Electron-electron interactions and spontaneous spin polarization in quantum Hall edge states. *Phys. Rev. Lett.* **70**, 3639–3642 (1993).
44. A. K. Evans, L. I. Glazman, B. I. Shklovskii, Coulomb blockade in the quantum-Hall-effect state. *Phys. Rev. B* **48**, 11120–11127 (1993).
45. N. C. van der Vaart, M. P. de Ruyter van Steveninck, L. P. Kouwenhoven, A. T. Johnson, Y. V. Nazarov, C. J. P. M. Harmans, C. T. Foxon, Time-resolved tunneling of single electrons between Landau Levels in a quantum dot. *Phys. Rev. Lett.* **73**, 320–323 (1994).
46. N. C. van der Vaart, L. P. Kouwenhoven, M. P. de Ruyter van Steveninck, Y. V. Nazarov, C. J. P. M. Harmans, C. T. Foxon, Time-resolved tunneling in the quantum Hall regime. *Phys. Rev. B* **55**, 9746–9756 (1997).
47. T. Heinzel, D. A. Wharam, J. P. Kotthaus, G. Böhm, W. Klein, G. Tränkle, G. Weimann, Periodic modulation of Coulomb-blockade oscillations in high magnetic fields. *Phys. Rev. B* **50**, 15113–15119 (1994).
48. A. Fuhrer, S. Lüscher, T. Heinzel, K. Ensslin, W. Wegscheider, M. Bichler, Transport properties of quantum dots with steep walls. *Phys. Rev. B* **63**, 125309 (2001).
49. J. C. Chen, M.-Y. Li, T. Ueda, S. Komiyama, Transport properties of a quantum dot in quantum Hall regimes probed by a single-electron transistor. *Appl. Phys. Lett.* **94**, 232109 (2009).
50. W. Liu, J. He, H. Guo, J. Gao, Electrochemical capacitance modulation in an interacting mesoscopic capacitor induced by internal charge transfer. *Phys. Rev. B* **97**, 165420 (2018).
51. M. Berl, L. Tiemann, W. Dietsche, H. Karl, W. Wegscheider, Structured back gates for high-mobility two-dimensional electron systems using oxygen ion implantation. *Appl. Phys. Lett.* **108**, 132102 (2016).
52. H. K. Choi, I. Sivan, A. Rosenblatt, M. Heiblum, V. Umansky, D. Mahalu, Robust electron pairing in the integer quantum hall effect regime. *Nat. Commun.* **6**, 7435 (2015).
53. I. Sivan, R. Bhattacharyya, H. K. Choi, M. Heiblum, D. E. Feldman, D. Mahalu, V. Umansky, Interaction-induced interference in the integer quantum Hall effect. *Phys. Rev. B* **97**, 125405 (2018).
54. S. Levy Schreier, A. Stern, B. Rosenow, B. I. Halperin, Thermodynamic properties of a quantum Hall anti-dot interferometer. *Physica E* **76**, 82–87 (2016).
55. A. H. MacDonald, Edge states in the fractional-quantum-Hall-effect regime. *Phys. Rev. Lett.* **64**, 220–223 (1990).
56. K. Lier, R. R. Gerhardts, Self-consistent calculations of edge channels in laterally confined two-dimensional electron systems. *Phys. Rev. B* **50**, 7757–7767 (1994).

Acknowledgments: We are thankful for the support of the ETH FIRST laboratory. **Funding:** We acknowledge financial support of the Swiss Science Foundation (Schweizerischer Nationalfonds, NCCR QSIT). B.R. would like to acknowledge support by DFG grant RO 2247/11-1. **Author contributions:** M.P.R. fabricated the devices and designed the experiments with supervision from T.I. and K.E. M.P.R. and M.H. performed the experiments and analyzed the data. G.N. and P.M. supported the experiments. C.R. and W.W. grew the semiconductor material. B.R. provided theoretical support. The manuscript was written by M.P.R. and revised by T.I., K.E., and B.R. with input of all authors. **Competing interests:** The authors declare that they have no competing interests. **Data and materials availability:** All data needed to evaluate the conclusions in the paper are present in the paper and/or the Supplementary Materials. The raw data and evaluation scripts used to generate the figures presented in this paper are available online at DOI: 10.3929/ethz-b-000455926. Additional data related to this paper may be requested from the authors.

Submitted 3 November 2020
Accepted 10 March 2021
Published 7 May 2021
10.1126/sciadv.abf5547

Citation: M. P. Rössli, M. Hug, G. Nicolí, P. Märki, C. Reichl, B. Rosenow, W. Wegscheider, K. Ensslin, T. Ihn, Fractional Coulomb blockade for quasi-particle tunneling between edge channels. *Sci. Adv.* **7**, eabf5547 (2021).